This article has been accepted for publication in a future issue of this journal, but has not been fully edited. Content may change prior to final publication. Citation information: DOI 10.1109/JSTARS.2021.3085556, IEEE Journal of Selected Topics in Applied Earth Observations and Remote Sensing

MODIS-Based Research on Secchi Disk Depth Using an Improved Semianalytical Algorithm in the Yellow Sea

Jie Zhan, Dianjun Zhang, Guoqing Zhou, Guangyun Zhang, Lingjuan Cao, and Quan Guo

***Abstract*—Secchi disk depth is a commonly measured parameter representing the optical properties of water bodies. Assessment of water transparency in seas is highly significant to marine-environment monitoring. In this study, an improved Secchi disk depth (Z_{SD}) inversion algorithm was proposed based on the Poole-Atkins model by determining the parameter A in the original model. The Forel-Ule Index (FUI) is a water color parameter that can be obtained from remote sensing data. Through the analysis of the International Ocean Color Coordinating Group (IOCCG) data set, it was found that there are strong logarithmic and quadratic correlations between the FUI and parameter A, whose R^2 values are 0.929 and 0.925, respectively. Comparing the results derived from MODIS product data with the in situ measured data in the Yellow Sea showed that the RMSE and MRE of the quadratic formula are 1.83 m and 43.74%, respectively, which reflect better performance than the other empirical formulas. Thus, parameter A can be expressed in quadratic form with FUI as a variable. Finally, we mapped the Z_{SD} inversion results for the Yellow Sea and analyzed the spatial changes. This study provides new insight for inverting Z_{SD} transparency algorithms and highlights the value of marine transparency monitoring.**

***Index Terms*—Secchi disk depth; MODIS; FUI (Forel-Ule Index); Yellow Sea**

I. Introduction

Secchi disk depth is a first-order indicator of marine water quality. It is related to the content of chlorophyll, suspended particles and gelbstoff in seawater, solar radiation on the sea surface and meteorological conditions. Monitoring the temporal and spatial variation in seawater transparency is of great significance to the study of seawater's physical and chemical properties, fishery production and naval military activities. The traditional method to measure the transparency of seawater is to use a Secchi disk on the ship for field measurements [1], [2]. However, this method can only yield Secchi disk depth values at the measurement points, which makes it impossible to obtain a larger spatial-temporal distribution of seawater transparency characteristics and cannot meet the needs of real-time monitoring of seawater transparency. With the development of ocean color remote sensing technology, and especially with the improvement of remote sensor performance, atmospheric correction technology and accuracy of water color information extraction modeling, real-time and large-scale satellite remote sensing monitoring of seawater transparency has become possible [3]-[5].

Seawater can be divided into Case I water and Case II water according to different optical properties. Case II water is mainly distributed in coastal and estuarine areas, which are most closely related to human beings and severely affected by human activities. The Yellow Sea is typical Case II water, and the optical properties of this sea area are very different and vary greatly with season. D. Yu et al [6] used a three-band algorithm to retireve Z_{SD} of the Yellow Sea based on remote sensing reflectance bands of 488, 555 and 678nm with a determination coefficient of 0.72 and a mean relative error of 19%. And Y. Mao et al [7] derived Z_{SD} from Geostationary Ocean Color Imager (GOCI) using a regional tuned model with a determination coefficient of 0.9 and mean absolute percent error of 24.56%. Overall, the previous inversion results did not reach desired accuracy. Therefore, it is necessary to develop a specific water transparency retrieval algorithm for the Yellow Sea, and the study of regional models will contribute to the further development of global Case II water transparency remote sensing.

The research on the water transparency inversion began in the 1970s. The CZCS (Costal Zone Color Scanner) carried by the Nimbus-7 satellite launched in 1978 was applied to remote sensing detection of the water transparency. Binding [8] established a linear estimation model for the water transparency of the Erie Lake in the United States by using CZCS's 550nm and SeaWiFS (Sea ViewingWideField of ViewSensor)'s 555nm reflectivity. With the deepening of the related research, more and more water transparency inversion algorithms had appeared. These algorithms can be classified into empirical

Manuscript received ; revised ; accepted
Date of publication ; date of current version
This work was supported by the National Key R&D Program of China (2018YFC1407400) and the National Natural Science Foundation of China (No.51678391) (*Corresponding author: Dianjun Zhang.*)

Jie Zhan, Dianjun Zhang, lingjuan Cao and Quan Guo are with the School of Marine Science and Technology, Tianjin University, Tianjin 300072, China (email: Zhanjie_2019@tju.edu.cn; zhangdianjun123@163.com; 2020227020@tju.edu.cn; gq341300@tju.edu.cn)

Guoqing Zhou is with Guangxi Key Laboratory for Spatial Information and Geomatics, Guilin University of Technology, Guilin, 541004, P. R. China. (gzhou@glut.edu.cn)

Guangyun Zhang is with School of Geomatics Science and Technology, Nanjing Tech University, Nanjing 211816, China(gyzhang1234@163.com)

This work is licensed under a Creative Commons Attribution 4.0 License. For more information, see https://creativecommons.org/licenses/by/4.0/

This article has been accepted for publication in a future issue of this journal, but has not been fully edited. Content may change prior to final publication. Citation information: DOI 10.1109/JSTARS.2021.3085556, IEEE Journal of Selected Topics in Applied Earth Observations and Remote Sensing

algorithms, semianalytical algorithms, analytical algorithms and machine learning algorithms [9]-[11]. Among them, the semianalytical algorithm is based on the theories of underwater light radiative transmission. It calculates the absorption coefficient and scattering coefficient of water components through remote sensing reflectance and constructs the relationship between measured transparency data and inherent optical properties to estimate seawater transparency. This method has good physical interpretation and applicability. However, some uncertain parameters in the model are usually obtained using empirical or semianalytical methods, which affects the accuracy of the model.

Based on the semianalytical algorithm, Tyler [12]-[15] and Preisendorfor [16]-[18] studied the relationship between water transparency and water optical parameters. They concluded that the transparency mainly depends on the inherent optical properties of the water without considering the effect of the measurement environment and the observers. On this basis, Doron et al. [19] established a quasi-analytical estimation model of water transparency based on the diffuse attenuation coefficient and beam attenuation coefficient at 490 nm. They also used 709 nm as the reference wavelength and the quasi-analytical algorithm (QAA) proposed by Lee et al. [20],[21] to calculate the diffuse attenuation coefficient and beam attenuation coefficient at 490 nm. Lee et al. [22] proposed an underwater visibility theory in 2015, which abandoned the traditional semianalytical algorithm by establishing the relationship between the sum of the diffuse attenuation coefficient and both the beam attenuation coefficient and water transparency. The new theory is reestablished, and the accuracy of the model is verified by 338 measured seawater transparency point data. The correction coefficient reaches 0.96, which greatly improves the accuracy of the semianalytical algorithm.

Although seawater transparency inversion algorithms have made great progress, there are still some problems to be solved. In the current inversion models, there are some undetermined parameters. Previous studies are used to determine the undetermined parameters based on the measured transparency data of Case II water in Europe and regard it as a constant. In fact, for different water qualities, we need to use different parameters to participate in the calculation. The Forel-Ule Index (FUI) and angle (α) have been shown to be useful water color parameters in indicating changes in water quality and can be derived from remote sensing data with high accuracies [23]-[25]. In this study, to improve the accuracy of transparency inversion models, the FUI index is introduced to determine the uncertain parameters in different water bodies. In the process of determining the parameters, it is necessary to calculate the value of FUI corresponding to the angle (α) through chromaticity coordinate calculations. Then, according to the formula for calculating the transparency, the FUI value is fitted with the measured transparency, and the final empirical formula of parameters is obtained. In this way, both the physical meaning of the semianalytical algorithm and the inversion accuracy can be ensured.

Section 2 introduces the Poole-Atkins Model and the Forel-Ule Index, and the study area and data are described in Section 3. Section 4 describes the model-building process, accuracy evaluation, and spatial analysis of the water transparency in the Yellow Sea and offers discussion. The conclusions are presented in Section 5.

II. METHOD

A. Poole-Atkins Model

The Poole-Atkins model compares water transparency with the change of underwater light field for the first time, and points out that water transparency is inversely proportional to the attenuation coefficient of water diffusion [26],[27]. This relationship can be obtained from the Lambert-Beer law.

$$E_d(SD) = E_d(0^-)\exp\left[-k_d \cdot SD\right] \quad (1)$$

$$SD = -\frac{ln\left[\frac{E_d(SD)}{E_d(0^-)}\right]}{k_d} \quad (2)$$

Lambert-Beer law only applied to narrow bands. Otherwise, the Lambert-Beer Law cannot be established due to the different attenuation coefficients of water diffusion for different wavebands.

Therefore, k_d in the formula (2) refer to the attenuation coefficient of the narrow waveband with the strongest penetrating ability in the water body. In the same way, $E_d(0^-)$ and $E_d(SD)$ also refer to the downward irradiance of the water subsurface and the depth of the Secchi disk of the narrow bands.

Let $A = ln\left[\frac{E_d(SD)}{E_d(0^-)}\right]$, then

$$SD = -\frac{A}{k_d} \quad (3)$$

That is, the transparency is inversely proportional to the diffuse attenuation coefficient of the narrow bands with the strongest penetrating ability in the water body. Robert. O. Megard & Tom Berman calculated $A \approx 1.54 \pm 0.13$ based on the transparency and underwater light field distribution data measured in the Southeast Mediterranean [28].

B. Forel-Ule Index

The Forel-Ule index (FUI) is one of the oldest and easiest measurements of water optical properties based on visual determinations, and it divides natural water color into 21 classes from dark blue to yellow-brown based on the Forel-Ule water color scale. Through remote sensing inversion algorithms, the Forel-Ule index can be obtained from remote sensing reflectance $R_{rs}(\lambda)$. Extracting water color parameters based on remote-sensing reflectance, the specific calculation process is as follows [24]:

(1) Use integrals to calculate X, Y, Z. Set the relative spectral energy distribution of the illuminating light source $S(\lambda)$ to 1. Then, substitute the remote sensing reflectance $R_{rs}(\lambda)$ into formula (4) as the spectral reflectance of the object $\rho(\lambda)$ and the product of the color matching function $\bar{x}(\lambda)$, $\bar{y}(\lambda)$ and $\bar{z}(\lambda)$ targeted in the visible light range (380 nm~700 nm) to obtain the CIE color tristimulus value. Among them, K is the adjustment factor.

$$X = K\int_{380}^{700} S(\lambda) \cdot \rho(\lambda) \cdot \bar{x}(\lambda)\, d\,\lambda$$

This work is licensed under a Creative Commons Attribution 4.0 License. For more information, see https://creativecommons.org/licenses/by/4.0/

This article has been accepted for publication in a future issue of this journal, but has not been fully edited. Content may change prior to final publication. Citation information: DOI 10.1109/JSTARS.2021.3085556, IEEE Journal of Selected Topics in Applied Earth Observations and Remote Sensing

$$Y = K\int_{380}^{700} S(\lambda)\cdot\rho(\lambda)\cdot\bar{y}(\lambda)\,d\lambda \quad (4)$$
$$Z = K\int_{380}^{700} S(\lambda)\cdot\rho(\lambda)\cdot\bar{z}(\lambda)\,d\lambda$$
$$K = 100/\int_{380}^{700} S(\lambda)\cdot\bar{y}(\lambda)\,d\lambda$$

(2) Calculate chromaticity coordinates (x, y). Substitute X, Y, Z into the formula (5) for normalization calculation to get x, y.

$$x = \frac{X}{X+Y+Z}$$
$$y = \frac{Y}{X+Y+Z} \quad (5)$$

(3) Calculate chromaticity angle α . Substitute the chromaticity coordinates (x, y) into the formula (6) to calculate the chromaticity angle α.

$$\alpha = ARCTAN2(y', x')$$
$$= ARCTAN2(x - 0.3333, y - 0.3333) \quad (6)$$

(4) Calculate the Forel-Ule index. Based on chromaticity angle α and the Forel-Ule index chromaticity lookup table, find the chromaticity value closest to α in the lookup table, and the Forel-Ule index corresponding to the chromaticity value is the water body's Forel-Ule water color index. The chromaticity coordinates, hue angle α of the Forel-Ule Scales are shown in table I.

TABLE I
THE CHROMATICITY COORDINATES, HUE ANGLE A OF THE FOREL-ULE SCALES

FUI	x	y	α	FUI	x	y	α
1	0.191363	0.166919	40.467	12	0.402416	0.4811	205.0622
2	0.198954	0.199871	45.19626	13	0.416243	0.47368	210.5766
3	0.210015	0.2399	52.85273	14	0.431336	0.465513	216.5569
4	0.226522	0.288347	67.16945	15	0.445679	0.457605	222.1153
5	0.245871	0.335281	91.29804	16	0.460605	0.449426	227.6293
6	0.266229	0.37617	122.5852	17	0.475326	0.440985	232.8302
7	0.290789	0.411528	151.4792	18	0.488676	0.43285	237.3523
8	0.315369	0.440027	170.4629	19	0.503316	0.424618	241.7592
9	0.336658	0.461684	181.4983	20	0.515498	0.416136	245.5513
10	0.363277	0.476353	191.8352	21	0.528252	0.408319	248.9529
11	0.386188	0.486566	199.0383				

C. Accuracy indexes

The root mean square error (RMSE), mean relative error (MRE) and R^2 are selected as the accuracy evaluation indicators for the water transparency inversion results. The RMSE is also called the standard error. It is the square root of the deviation between the observed value and the true value for n observations. The average relative error is the average value of the relative error, which is generally expressed by the absolute value of the average relative error [29]. $Z_{SD_i}^{\ D}$ in Equations (7) and (8) is the Secchi disk depth obtained by the inversion, and $Z_{SD_i}^{\ M}$ is the measured Secchi disk depth. R^2 is the ratio of the square of the regression to the sum of the total deviation squared. Higher model accuracy and more significant regression effects are indicated by larger ratios. The value of R^2 is between 0~1. The closer to 1, the better the regression fitting effect is.

$$RMSE = \left(\frac{1}{n-1}\sum_{i=1}^{n}\left[Z_{SD_i}^{\ D} - Z_{SD_i}^{\ M}\right]^2\right)^{0.5} \quad (7)$$
$$MRE = \left(\frac{1}{n}\sum_{i=1}^{n}\frac{|Z_{SD_i}^{\ D} - Z_{SD_i}^{\ M}|}{Z_{SD_i}^{\ M}}\right)\times 100\% \quad (8)$$

III. STUDY AREA AND DATA

A. Study Area

The Yellow Sea is the research area in this study, and it is located at 31.6-39.8°N, 119-126.8°E as a fringe sea in the western Pacific Ocean. It borders North Korea and South Korea to the east, China's Liaoning Province to the north, Shandong Province and Jiangsu Province to the west and Jeju Island to the south.

The winter temperature in the Yellow Sea is between -2~8°C, the lowest average temperature occurs in January, and the temperature difference between the north and south is large. In summer, due to solar radiation, the usual rainy season for the Yellow Sea is from June to August, and rainfall during this period can account for 50% to 70% of the total annual rainfall. In this period, the temperature generally rises, and the surface water temperature is between 24~27°C. The turbidity of the water in this study area has significant variability.

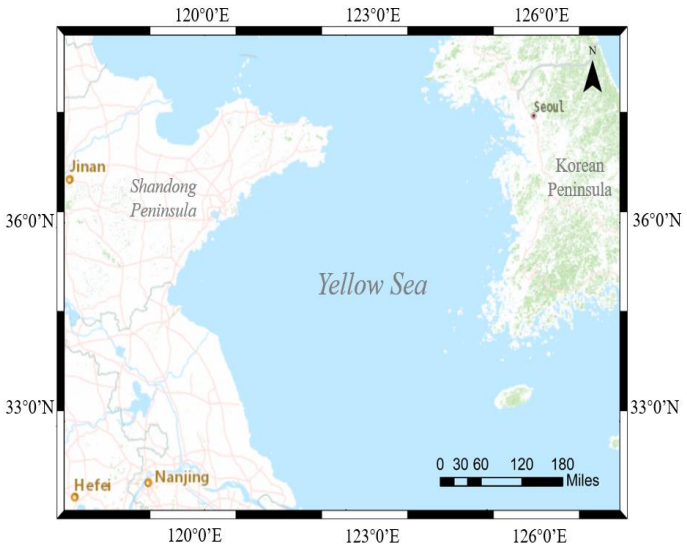

Fig. 1. Map of study area

This work is licensed under a Creative Commons Attribution 4.0 License. For more information, see https://creativecommons.org/licenses/by/4.0/

This article has been accepted for publication in a future issue of this journal, but has not been fully edited. Content may change prior to final publication. Citation information: DOI 10.1109/JSTARS.2021.3085556, IEEE Journal of Selected Topics in Applied Earth Observations and Remote Sensing

B. Data

1) MODIS Data

MODIS ocean color products (https://oceancolor.gsfc.nasa.gov/) provide spectral reflectance for bands 1-6 (i.e., 412, 443, 490, 555, 660 and 680 nm) and diffuse attenuation coefficient $k_d(490)$ at 490 nm with a spatial resolution of 500 m. The product data are an important data source for long-term and large-scale marine-environment monitoring [22]. The ocean color data of the Yellow Sea in August and November 2016 were downloaded from the NASA website to match the *in situ* data and develop the model.

2) In Situ Data

Two samplings were conducted in August and November 2016. There were 47 sampling points each month. The sampling points in these two months were exactly the same, for a total of 94 sampling points. The geographical location sampled is 36°18'48"~ 36°36'33"N, 121°00'43"~ 121°51'44"E, mainly distributed along the southeastern Shandong Peninsula. The sampling point distribution is shown in Fig. 2. Partial transparency measured data are shown in table II. The in situ measured Z_{SD} data were matched up with monthly MODIS product data for the purpose of developing a water transparency inversion algorithm.

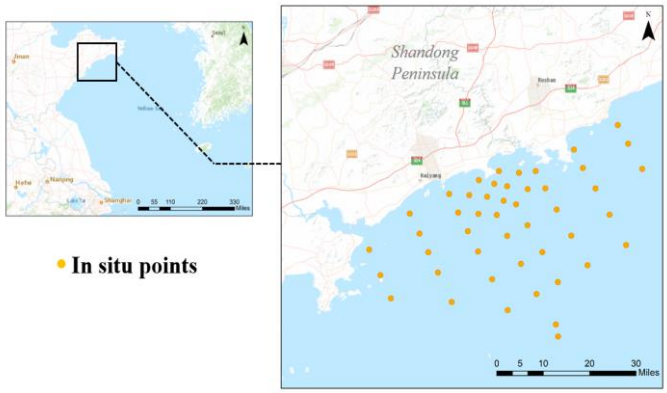

Fig. 2. Sampling distribution

Table II
Partial transparency measured data

Site name	Lat(N)	Lon(E)	Date	Z_{SD}(m)
1	36.52436	121.0119	2016.8.14	2.5
2	36.40623	121.0794	2016.8.14	4
3	36.39723	121.2686	2016.8.14	5
4	36.72018	121.8621	2016.8.14	1.5
5	36.7226	121.6776	2016.8.14	0.6
6	36.61443	121.2889	2016.11.16	1
7	36.51999	121.3507	2016.11.16	1.7
8	36.37733	121.443	2016.11.16	2.3
9	36.55832	121.6411	2016.11.16	1.5
10	36.76694	121.6496	2016.11.16	0.6

3) IOCCG Data

In addition to the *in situ* dataset, the Hydrolight simulated IOCCG dataset (https://www.ioccg.org/data/ioccg2010_simulated_data.d/) consists of 500 data points. IOCCG data set is obtained from radiative transfer simulation, at 30°sun zenith, of synthesized inherent optical properties (IOPs). IOCCG spectra were simulated assuming the solar irradiance model of Gregg and Carder and a cloud-free sky [30]. It includes the remote sensing reflectance R_{rs},the absorption a, and the backscattering coefficient, b_b, in the range of 400 nm to 800 nm. In this study, the IOCCG dataset was employed to develop the water transparency inversion algorithm and analyze the applicability of the model. In the dataset, the Forel-Ule index can be calculated from R_{rs}. The Z_{SD} of each simulation can be derived by the method proposed by Lee et al. [23].

IV. Results and Discussion

A. Z_{SD} model development

Previous studies did not produce a universal method to determine the parameters A in the Poole-Atkins Model. Different studies have reported different values of A. Through the analysis of the IOCCG data set, we found that there is a strong correlation between the undetermined parameters A and the Forel-Ule index, which means that parameter A should not always be a constant but a variable that changes constantly according to variations in water quality. However, the Forel-Ule index, as a water color index, can reflect the water quality of different water bodies to a large extent.

The IOCCG dataset, a Hydrolight simulated dataset, is used to analyze the relationship between the Forel-Ule index and parameter A in this study. The dataset provided the diffuse attenuation coefficient k_d, and we can calculate Z_{SD} from the dataset through the method proposed by Lee et al. Then, according to formula (3), we can obtain the value of A. The Forel-Ule index can also be calculated from the remote sensing reflectance R_{rs} at wavelengths of 450 nm, 550 nm and 650 nm in the IOCCG dataset. The distribution of the calculated FUI (0-16) is shown in Fig. 3. Finally, we obtain 500 sets of FUI and parameter A corresponding to each other. To better analyze the relationship between the FUI and the undetermined parameter A, we removed the values of A when the FUI was equal to 15 and 16 for a small amount of data and took the average of the A corresponding to each FUI value from 1 to 14. The results are shown in the table III.

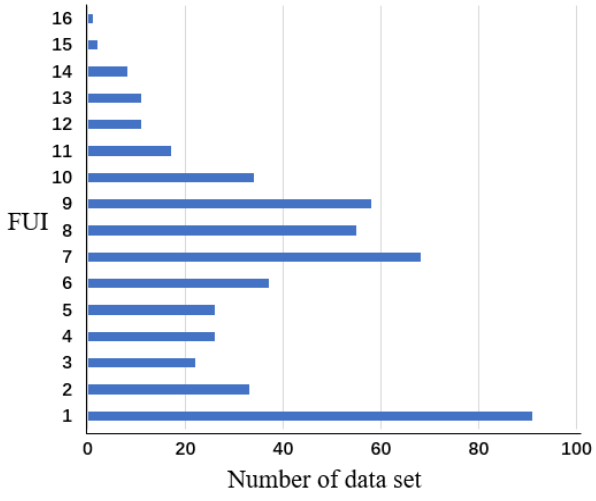

Fig. 3. Number of data sets corresponding to different FUI

This work is licensed under a Creative Commons Attribution 4.0 License. For more information, see https://creativecommons.org/licenses/by/4.0/

This article has been accepted for publication in a future issue of this journal, but has not been fully edited. Content may change prior to final publication. Citation information: DOI 10.1109/JSTARS.2021.3085556, IEEE Journal of Selected Topics in Applied Earth Observations and Remote Sensing

Table III
FUI and Corresponding average undermined parameters (A) table

FUI	1	2	3	4	5	6	7
A(Average)	1.0492	0.8662	0.7603	0.7553	0.6864	0.6711	0.6238
FUI	8	9	10	11	12	13	14
A(Average)	0.6084	0.5771	0.6242	0.5972	0.5883	0.5929	0.6021

Next, we analyzed the relationship between the simulated FUI and parameter A and found that there was a strong correlation between these two parameters. Linear formulas, quadratic formulas, exponential formulas, and logarithmic formulas were used in the process of data analysis. In addition, the fitting results are shown in Fig. 4. The poor results of exponential fitting showed a correlation coefficient R^2 of only 0.74. The linear fitting and quadratic fitting results are better than the exponential fitting, and R^2 reached 0.88 and 0.93, respectively. The logarithmic fit yields the best result with an R^2 of approximately 0.93. Therefore, the water transparency inversion formula can be developed as follows:

$$A=f(FUI),\ Z_{SD}=\frac{f(FUI)}{k_d} \quad (9)$$

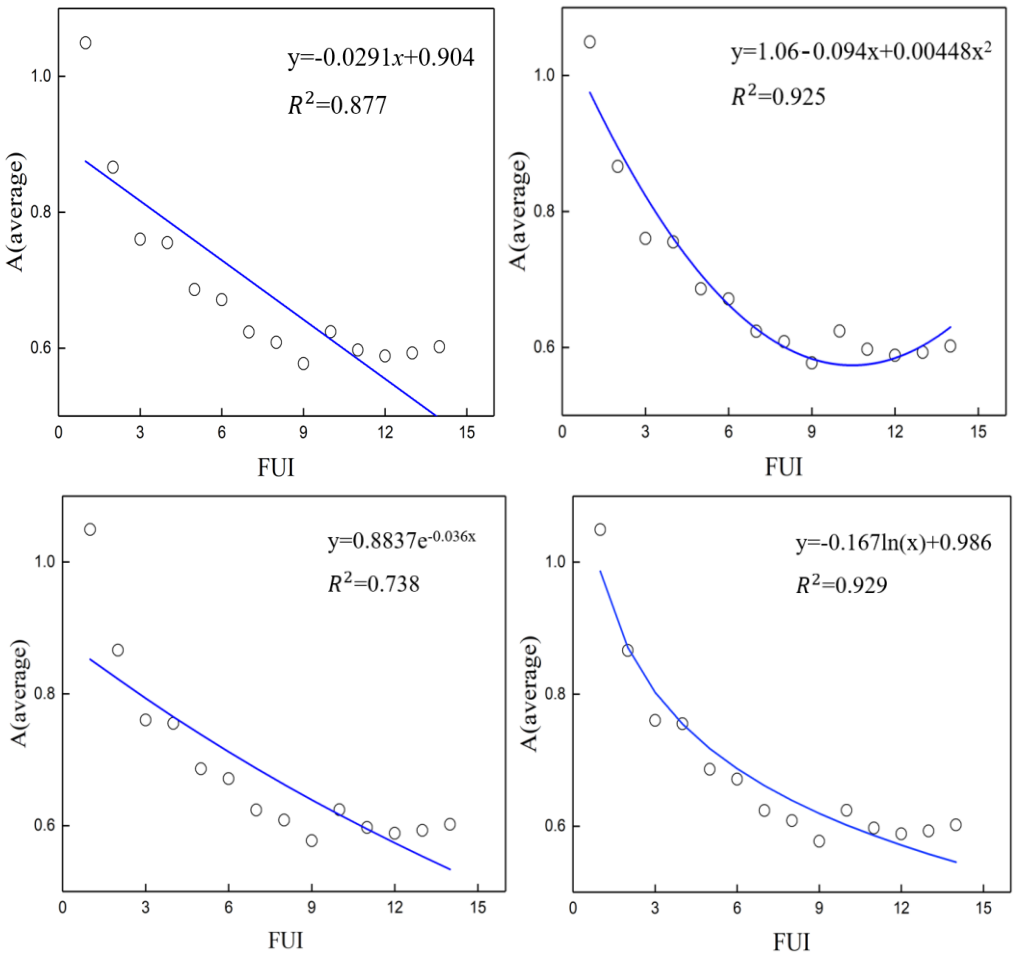

Fig. 4. Scatterplots of parameters A (average) and FUI based on the IOCCG dataset

B. *Model validation*

After developing a new model by analyzing the IOCCG dataset, it is necessary to use measured data to verify and evaluate the accuracy y of the established model. In this study, MODIS product data were selected to retrieve water transparency with the new model. First, the hue angle α can be calculated from the remote sensing reflectance at 450 nm, 550 nm, and 650 nm. Based on the chromaticity coordinates table, we can obtain the hue angle α. For eliminating the error caused by the MODIS, we corrected the obtained hue angle, and the α comparison before and after correction is shown in Figure 5.

The MODIS product data also include the diffuse attenuation coefficient at 490 nm, $k_d(490)$. Then, based on the proposed formula, we can obtain the derived Secchi disk depth, which should be compared with the measured data. The processing flow for MODIS data is shown in Fig. 6.

When parameter A is expressed in linear, quadratic, logarithmic and exponential formulas, and the dependent variable is FUI, four sets of the derived water transparency values are obtained. The four sets of water transparency values are compared and analyzed with the in-situ transparency values. And the analysis results are shown in Fig. 7. and table IV.

This work is licensed under a Creative Commons Attribution 4.0 License. For more information, see https://creativecommons.org/licenses/by/4.0/

This article has been accepted for publication in a future issue of this journal, but has not been fully edited. Content may change prior to final publication. Citation information: DOI 10.1109/JSTARS.2021.3085556, IEEE Journal of Selected Topics in Applied Earth Observations and Remote Sensing

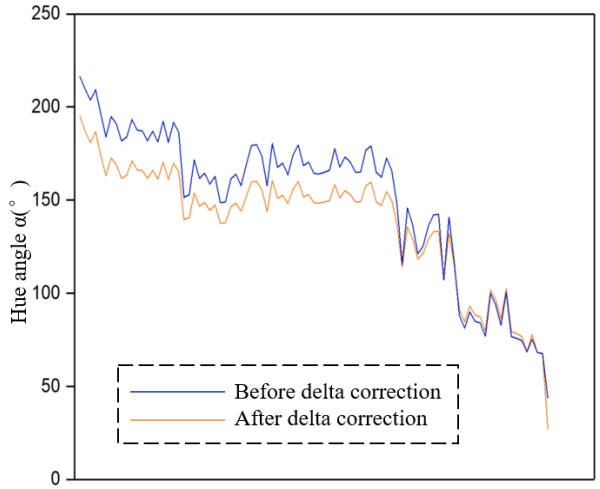

Fig. 5. The chromaticity angle α before and after correction

Fig. 7. illustrates that the overall inversion results are a little larger than the measured data. And there is not much difference between the four inversion results. However, from the error analysis table of the developed model, we can conclude that the quadratic fitting performs better than the other fitting formulas with the RMSE and MRE are 1.83 and 43.74% respectively. And inversion accuracy of the developed model is much higher than the traditional inversion algorithm proposed by Robert O. Megard & Tom Berman (A is always equal to 1.54) [26]. Therefore, the formula can be written as the formula (10).

$$Z_{SD}=\frac{1.06-0.094\times FUI+0.00448\times FUI^2}{k_d} \quad (10)$$

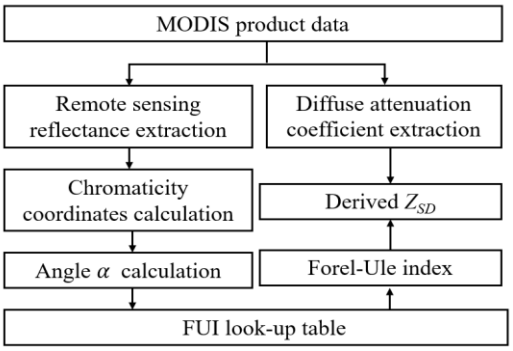

Fig. 6. The flow chart for MODIS data processing

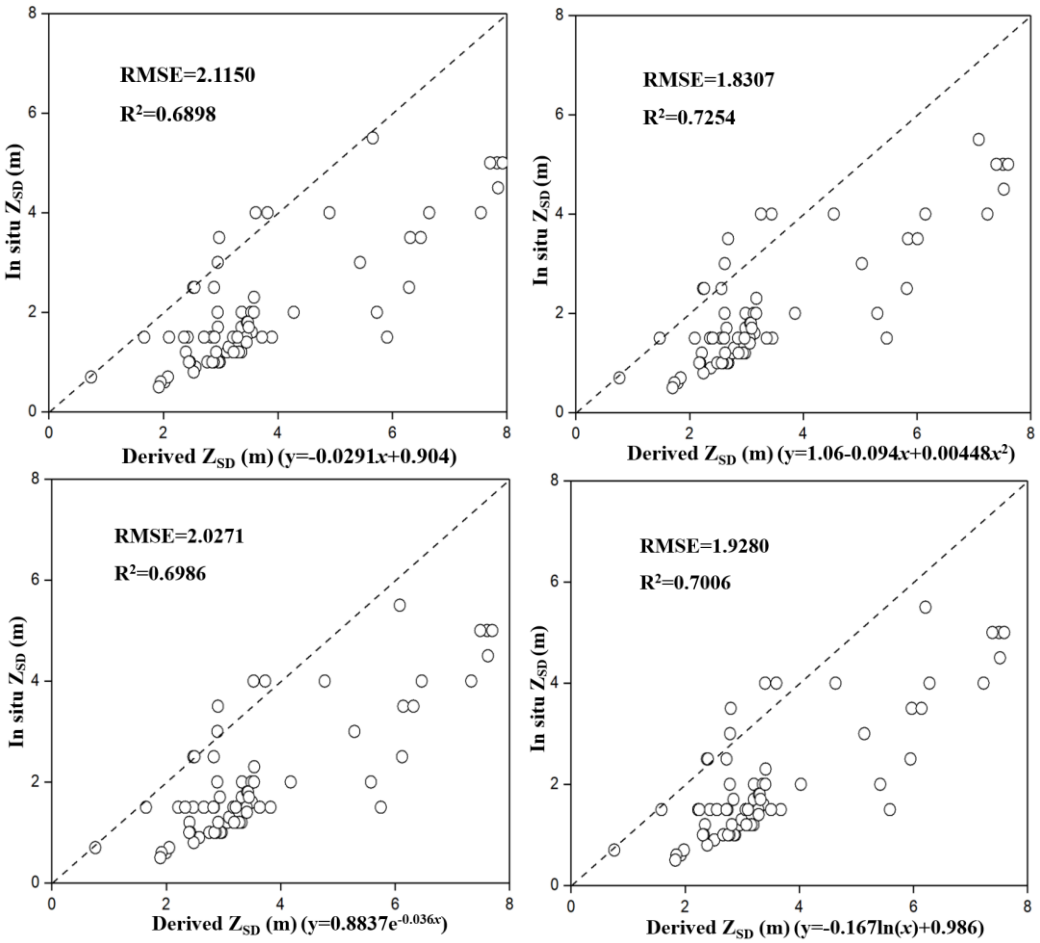

Fig.7. Scatterplots of the in-situ measured Z_{SD} and MODIS derived Z_{SD}

This work is licensed under a Creative Commons Attribution 4.0 License. For more information, see https://creativecommons.org/licenses/by/4.0/

This article has been accepted for publication in a future issue of this journal, but has not been fully edited. Content may change prior to final publication. Citation information: DOI 10.1109/JSTARS.2021.3085556, IEEE Journal of Selected Topics in Applied Earth Observations and Remote Sensing

Table IV
Error analysis table of the developed model

Formula	linear	quadratic	exponential	logarithmic	$1.54/k_d$
RMSE	2.1150	1.8307	2.0271	1.9280	6.6115
MRE	46.63%	43.74%	46.24%	45.25%	74.64%
R^2	0.6898	0.7254	0.6986	0.7047	0.7006

C. Spatial patterns of water transparency across the Yellow Sea

The MODIS product data were selected as the remote sensing data source in this study, which is suitable for water transparency mapping in the Yellow Sea. The dataset used for mapping is from September 22 with fewer clouds and sufficient data. The developed model is used in the inversion process, and the inversion result is colored and shown in Fig. 8. The figure shows that the Secchi disk depth of the Yellow Sea ranges from 0 to 17.383 meters with an average value of approximately 7.573m. Moreover, it is easy to find that the Secchi disk depth of the water body in coastal waters is low, most of which is below 10 m. However, as far from the shore, the value of water transparency also increases significantly. The water transparency value of the central sea area can reach more than 12 m. In general, the northeastern part of the Yellow Sea is slightly more transparent than the southwestern part.

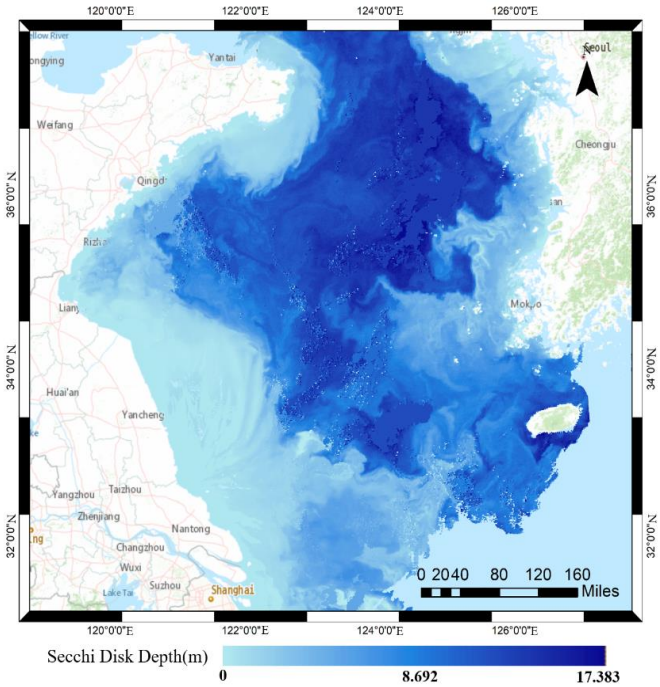

Fig. 8. Z_{SD} Inversion results mapping of the Yellow Sea in September 22

D. Discussion

1) Factors affecting inversion results

First, the MODIS product data used in the research have a low resolution: 1000 m per pixel. It is difficult to ensure that the water transparency value of 1 square kilometer is the same, which will affect the accuracy of the remote sensing inversion results. In future research, it will be necessary to use higher-resolution remote sensing images.

Second, the Yellow Sea is a typical case II water body. The coastal area has frequent human activities and serious pollution. Therefore, the water transparency value is extremely low, and some may be less than 1 m; thus, the relative error of the inversion will be greatly increased.

2) Algorithm uncertainties

In this study, we have proposed a new idea to solve the parameter A in the Poole-Atkins model, and the developed method has strong applicability and can be applied to different waters. In the process of verifying the model with measured data, it is found that the accuracy of the new model is indeed higher than that of the traditional method, but it still has not reached a high level of accuracy. In the follow-up, more measured data for different seas should be involved to improve and validate the model.

Moreover, satellite remote sensing data should be effectively combined with ground measured data. Therefore, a simple and effective atmospheric-correction algorithm based on current sensor technology should be studied and developed for near-shore water bodies [31]-[35].

The determination of parameter A in the developed model still adopted the empirical method. The Secchi disk depth inversion methods and techniques should be further optimized to improve the inversion efficiency and analyzed to develop theoretical models with rigorous derivation processes and robust physical mechanisms.

3) Factors affecting water transparency

The transparency of seawater is one of the water quality evaluation indicators. The main factors affecting the transparency of seawater are the height of the sun, the concentration of suspended solids and plankton et al. Generally, the greater the sun's altitude angle, the greater the amount of light entering the lake and the greater the transparency, and vice versa. In the same way, the more suspended matter and plankton in the lake water, the stronger the scattering and absorption of light, and the lower the transparency.

V. Conclusions

The In this study, we improved the Poole-Atkins model to estimate Z_{SD} for the Yellow Sea of China based on the hydrolight simulated dataset IOCCG dataset and verified the accuracy of the developed model based on the measured Secchi disk depth data and synchronous MODIS product data.

By analyzing the IOCCG dataset, we found that the parameter A in the Poole-Atkins model should not be always constant. However, when the Forel-Ule index is different, the parameter A should also be changed, in order to ensure the Z_{SD} inversion accuracy. In other words, there is a good correlation between the FUI and the undetermined parameter A. Through analysis, the logarithmic and quadratic fitting results are better than the linear and exponential relationship.

When comparing with the measured data, it is found that the

This work is licensed under a Creative Commons Attribution 4.0 License. For more information, see https://creativecommons.org/licenses/by/4.0/

This article has been accepted for publication in a future issue of this journal, but has not been fully edited. Content may change prior to final publication. Citation information: DOI 10.1109/JSTARS.2021.3085556, IEEE Journal of Selected Topics in Applied Earth Observations and Remote Sensing

exponential fit is the best, and the accuracy of the new model is greatly improved compared with the traditional model (A is a constant). Therefore, the inversion formula of the new model can be determined.

Based on the Z_{SD} inversion results mapping of the Yellow Sea, we can conclude that the water transparency of the sea center is higher than that of coastal waters. And some areas along the coast have extremely low transparency, which require the government to control marine pollution to reduce the impact of human activities.

In the future, more research on water transparency is needed for water quality conservation and management. And it is important to highlight the value of satellite remote sensing in monitoring water quality at large scale and over long term.

REFERENCES

[1] J. R. V. Zaneveld, and W. S. Pegau, "Robust underwater visibility parameter," *Opt Express.*, vol. 11, no. 23, pp. 2997-3009, 2003.

[2] X. He, D. Pan, Y. Bai, T. Wang, C.-T. A. Chen, Q. Zhu, Z. Hao, and F. Gong, "Recent changes of global ocean transparency observed by SeaWiFS," *Cont. Shelf Res.*, vol. 143, pp. 159-166, 2017.

[3] X. Liu, Z. Lee, Y. Zhang, J. Lin, K. Shi, Y. Zhou, B. Qin, and Z. Sun, "Remote sensing of secchi depth in highly turbid lake waters and its application with MERIS data," *Remote Sens.*, vol. 11, no. 19, pp. 2226, 2019.

[4] Y. Bai, X. He, S. Yu, and C.-T. A. Chen, "Changes in the Ecological Environment of the Marginal Seas along the Eurasian Continent from 2003 to 2014," *Sustainability.*, vol. 10, no. 3, pp. 635, 2018.

[5] M. R. Lewis, N. Kuring, and C. Yentsch, "Global patterns of ocean transparency: Implications for the new production of the open ocean," *J. of Geophys Res: Oceans.*, vol. 93, no. C6, pp. 6847-6856, 1988.

[6] D. Yu, Q. Xing, M. Lou, and P. Shi, "Retrieval of Secchi disk depth in the Yellow Sea and East China Sea using 8-day MODIS data." p. 012112.

[7] Y. Mao, S. Wang, Z. Qiu, D. Sun, and M. Bilal, "Variations of transparency derived from GOCI in the Bohai Sea and the Yellow Sea," *Opt Express.*, vol. 26, no. 9, pp. 12191-12209, 2018.

[8] C. E. Binding, J. H. Jerome, R. P. Bukata, and W. G. Booty, "Trends in water clarity of the lower Great Lakes from remotely sensed aquatic color," *J. Great Lakes Res.*, vol. 33, no. 4, pp. 828-841, 2007.

[9] C. E. Binding, J. H. Jerome, R. P. Bukata, and W. G. Booty, "Trends in water clarity of the lower Great Lakes from remotely sensed aquatic color," *J. Great Lakes Res.*, vol. 33, no. 4, pp. 828-841, 2007.

[10] M. Shen, H. Duan, Z. Cao, K. Xue, T. Qi, J. Ma, D. Liu, K. Song, C. Huang, and X. Song, "Sentinel-3 OLCI observations of water clarity in large lakes in eastern China: Implications for SDG 6.3. 2 evaluation," *Remote Sens. Environ.*, vol. 247, pp. 111950, 2020.

[11] M. Doron, M. Babin, O. Hembise, A. Mangin, and P. Garnesson, "Ocean transparency from space: Validation of algorithms estimating Secchi depth using MERIS, MODIS and SeaWiFS data," *Remote Sens. Environ.*, vol. 115, no. 12, pp. 2986-3001, 2011.

[12] J. E. Tyler, "The secchi disc," *Limnol. Oceanogr.*, vol. 13, no. 1, pp. 1-6, 1968.

[13] N. Chang, L. Luo, X. C. Wang, J. Song, J. Han, and D. Ao, "A novel index for assessing the water quality of urban landscape lakes based on water transparency," *Sci. Total Environ.*, vol. 735, pp. 139351, 2020.

[14] T. Rodrigues, E. Alcântara, F. Watanabe, and N. Imai, "Retrieval of Secchi disk depth from a reservoir using a semi-analytical scheme," *Remote Sens. Environ.*, vol. 198, pp. 213-228, 2017.

[15] K. Alikas, and S. Kratzer, "Improved retrieval of Secchi depth for optically-complex waters using remote sensing data," *Ecol. Indic.*, vol. 77, pp. 218-227, 2017.

[16] R. W. Preisendorfer, "Secchi disk science: Visual optics of natural waters 1," *Limnol. Oceanogr.*, vol. 31, no. 5, pp. 909-926, 1986.

[17] I. Chawla, L. Karthikeyan, and A. K. Mishra, "A review of remote sensing applications for water security: Quantity, quality, and extremes," *J. Hydrol.*, vol. 585, pp. 124826, 2020.

[18] K. Song, G. Liu, Q. Wang, Z. Wen, L. Lyu, Y. Du, L. Sha, and C. Fang, "Quantification of lake clarity in China using Landsat OLI imagery data," *Remote Sens. Environ.*, vol. 243, pp. 111800, 2020.

[19] M. Doron, M. Babin, A. Mangin, and O. Hembise, "Estimation of light penetration, and horizontal and vertical visibility in oceanic and coastal waters from surface reflectance," *J. Geophys. Res.: Oceans.*, vol. 112, no. C6, 2007.

[20] Z. Lee, K. L. Carder, and R. A. Arnone, "Deriving inherent optical properties from water color: a multiband quasi-analytical algorithm for optically deep waters," *Appl. Opt.*, vol. 41, no. 27, pp. 5755-5772, 2002.

[21] Z. P. Lee, M. Darecki, K. L. Carder, C. O. Davis, D. Stramski, and W. J. Rhea, "Diffuse attenuation coefficient of downwelling irradiance: An evaluation of remote sensing methods," *J. Geophys. Res.: Oceans.*, vol. 110, no. C2, 2005.

[22] Z. Lee, S. Shang, C. Hu, K. Du, A. Weidemann, W. Hou, J. Lin, and G. Lin, "Secchi disk depth: A new theory and mechanistic model for underwater visibility," *Remote Sens. Environ.*, vol. 169, pp. 139-149, 2015.

[23] H. J. Van der Woerd, and M. R. Wernand, "Hue-angle product for low to medium spatial resolution optical satellite sensors," *Remote Sens.*, vol. 10, no. 2, pp. 180, 2018.

[24] S. Wang, J. Li, B. Zhang, Z. Lee, E. Spyrakos, L. Feng, C. Liu, H. Zhao, Y. Wu, and L. Zhu, "Changes of water clarity in large lakes and reservoirs across China observed from long-term MODIS," *Remote Sens. Environ.*, vol. 247, pp. 111949, 2020.

[25] S. P. Garaba, A. Friedrichs, D. Voß, and O. Zielinski, "Classifying natural waters with the Forel-Ule Colour index system: results, applications, correlations and crowdsourcing," *Int. J. Environ. Res. Public Health.*, vol. 12, no. 12, pp. 16096-16109, 2015.

[26] H. Poole, and W. Atkins, "Photo-electric measurements of submarine illumination throughout the year," *J. Mar. Biol. Assoc. U. K.*, vol. 16, no. 1, pp. 297-324, 1929.

[27] P. J. Lisi, and C. L. Hein, "Eutrophication drives divergentwater clarity responses to decadal variation in lake level," *Limnol. Oceanogr.*, vol. 64, no. S1, pp. S49-S59, 2019.

[28] R. O. Megard, and T. Berman, "Effects of algae on the Secchi transparency of the southeastern Mediterranean Sea," *Limnol. Oceanogr.*, vol. 34, no. 8, pp. 1640-1655, 1989.

[29] C. J. Willmott, and K. Matsuura, "Advantages of the mean absolute error (MAE) over the root mean square error (RMSE) in assessing average model performance," *Clim. Res.*, vol. 30, no. 1, pp. 79-82, 2005.

[30] W. W. Gregg, and K. L. Carder, "A simple spectral solar irradiance model for cloudless maritime atmospheres," *Limnol. Oceanogr*, vol. 35, no. 8, pp. 1657-1675, 1990.

[31] L. Feng, X. Hou, and Y. Zheng, "Monitoring and understanding the water transparency changes of fifty large lakes on the Yangtze Plain based on long-term MODIS observations," *Remote Sens. Environ.*, vol. 221, pp. 675-686, 2019.

[32] Z. Lee, S. Shang, K. Du, and J. Wei, "Resolving the long-standing puzzles about the observed Secchi depth relationships," *Limnol. Oceanogr.*, vol. 63, no. 6, pp. 2321-2336, 2018.

This work is licensed under a Creative Commons Attribution 4.0 License. For more information, see https://creativecommons.org/licenses/by/4.0/

This article has been accepted for publication in a future issue of this journal, but has not been fully edited. Content may change prior to final publication. Citation information: DOI 10.1109/JSTARS.2021.3085556, IEEE Journal of Selected Topics in Applied Earth Observations and Remote Sensing

[33] Z. Cao, R. Ma, H. Duan, and K. Xue, "Effects of broad bandwidth on the remote sensing of inland waters: Implications for high spatial resolution satellite data applications," *ISPRS J. Photogra and Remote Sensi.*, vol. 153, pp. 110-122, 2019.

[34] W. Yang, B. Matsushita, J. Chen, K. Yoshimura, and T. Fukushima, "Application of a semianalytical algorithm to remotely estimate diffuse attenuation coefficient in turbid inland waters," *IEEE Geosci. Remote Sens. Lett.*, vol. 11, no. 6, pp. 1046-1050, 2013.

[35] C. F. Le, Y. M. Li, Y. Zha, D. Sun, and B. Yin, "Validation of a quasi-analytical algorithm for highly turbid eutrophic water of Meiliang Bay in Taihu Lake, China," *IEEE Trans. Geosci. Remote Sens.*, vol. 47, no. 8, pp. 2492-2500, 2009.

Jie Zhan was born in Yantai, Shandong, China, in 1997. She received the B.S. degree in geomatics engineering from Shandong University of science and technology, Qingdao, China, in 2019. She is currently pursuing the M.S. degree in School of Marine Science and Technology, Tianjin University. Her research interests include ocean color remote sensing and inversion algorithms.

Dianjun Zhang was born in Shandong, China, in 1986. He received the M.S. and Ph.D. degrees in geographical information system from Beijing Forestry University and the Institute of Geographic Sciences and Natural Resources Research, Chinese Academy of Sciences, China, in 2011 and 2015, respectively. His research interests include ocean remote sensing and ship recognition based on deep learning methods.

Guoqing Zhou (Senior Member, IEEE) received the Ph.D. degree from Wuhan University, Wuhan, China, in 1994. He was a Visiting Scholar with the Department of Computer Science and Technology, Tsinghua University, Beijing, China, and a Post-doctoral Researcher with the Institute of Information Science, Beijing Jiaotong University, Beijing, China. He continued his research as an Alexander von Humboldt Fellow with the Technical University of Berlin, Berlin, Germany, from 1996 to 1998, and was a Post-doctoral Researcher with The Ohio State University, Columbus, OH, USA, from 1998 to 2000. He was Assistant Professor, Associate Professor, and Full Professor with Old Dominion University, Norfolk, VA, USA, in 2000, 2005, and 2010, respectively. He has authored five books and more than 380 refereed papers.

Guangyun Zhang received the B.Sc. degree from the China University of Mining and Technology, Xuzhou, China, in 2007 and the Ph.D. degree in electrical engineering from the University of New South Wales, Sydney, Australia, in 2013. Since 2019, he has been with t School of Geomatics Science and Technology, Nanjing Tech University, Nanjing 211816, China, where he is currently a professor. He is also with the University of New South Wales, Canberra, Australia. His research interests include imaging spectrometry and LiDAR.

Lingjuan Cao. was born in Zhejiang, China, in 1997. She received the B.S. degree in North China University of Science and Technology, China, in 2020. She is currently pursuing the M.S. degree in School of Marine Science and Technology, Tianjin University. Her research interest is ocean mesoscale eddies with remote sensing.

Quan Guo was born in Jiangxi, China, in 1998. He received the Bachelor's Degree in Tianjin University, China, in 2020. He is currently pursuing the M.S. degree in School of Marine Science and Technology, Tianjin University. His research interest is the inversion of the three-dimensional temperature field using ocean remote sensing methods.

This work is licensed under a Creative Commons Attribution 4.0 License. For more information, see https://creativecommons.org/licenses/by/4.0/